

## Research article

# Fouling dynamics varied by filtration cycles in high-solid anaerobic membrane bioreactors for sewage sludge treatment



Hao-Jie Qin<sup>a</sup>, Ming Zhu<sup>b</sup>, Shenghao Ji<sup>a</sup>, Ruixin Wu<sup>b</sup>, Yuki Yamamoto<sup>a</sup>, Yu Qin<sup>a,\*</sup> , Yu-You Li<sup>a,b</sup>

<sup>a</sup> Department of Civil and Environmental Engineering, Graduate School of Engineering, Tohoku University, 6-6-06 Aoba, Aramaki-Aza, Sendai, Miyagi, 980-8579, Japan

<sup>b</sup> Department of Frontier Sciences for Advanced Environment, Graduate School of Environmental Studies, Tohoku University, 6-6-20 Aoba, Aramaki-Aza, Sendai, Miyagi, 980-8579, Japan

## ARTICLE INFO

### Keywords:

Anaerobic membrane bioreactors  
Filtration cycles  
Filtration/relaxation ratio  
Membrane fouling  
Power-law model

## ABSTRACT

Anaerobic membrane bioreactors (AnMBRs) are highly effective in treating sewage sludge (SewS) by promoting the rate-limiting hydrolysis process through biosolids concentration. The treatment of SewS in this study by the high-solid AnMBR achieved an exceptional COD removal efficiency of 99.1 % and a substantial bioenergy yield of 157.8 mL-CH<sub>4</sub>/g-COD<sub>add</sub>. However, membrane fouling remains a critical challenge, restricting the long-term stable operation of high-solid AnMBRs for SewS treatment. To address this challenge, membrane filtration performance was evaluated under various combinations of instantaneous flux and filtration/relaxation ratios (F/R). The optimal F/R was identified as 3:1 (min/min), effectively mitigating membrane fouling and maintaining a total resistance of at least  $7.20 \times 10^{12} \text{ m}^{-1}$ , where the flux maintenance efficiency of this filtration cycle peaked at 94.7 % for 4 h. An empirical model describing the relationship between filtrate volume and  $\Delta\text{TMP}$  was established as  $\ln(\Delta\text{TMP}) = k \cdot \ln(v) + b$ , exhibiting high coefficients of determination. The influence of filtration cycles on membrane fouling rates was analyzed through the power-law model. Furthermore, real-time transmembrane pressure (TMP) curves were utilized to identify fouling types based on the constant-flux filtration models ( $dp/dv = k'p^n$ ). Filtration cycles with high instantaneous flux (16.68–23.60 LMH) and extended relaxation periods (2–3 min) predominantly exhibited cake layer formation, whereas cycles with lower instantaneous flux (7.40–11.79 LMH) and shorter relaxation periods (1 min) were more prone to intermediate pore blocking. This study provides mechanistic insights into the optimization of filtration process in engineering applications, paving the way for the long-term sustainable operation of high-solid AnMBR systems.

## 1. Introduction

Primary sludge (PS) and waste activated sludge (WAS) from wastewater treatment plants (WWTPs) are rich in biodegradable organics such as carbohydrates and proteins, making them attractive substrates for renewable energy recovery (Geng et al., 2024; Tan et al., 2024). Anaerobic digestion (AD) is widely used for converting these organics into methane (Ye et al., 2024), but the hydrolysis of sewage sludge (SewS) remains a rate-limiting step due to its complex structure and low biodegradability (Wang et al., 2023a,b). Recent studies have shown that anaerobic membrane bioreactors (AnMBRs) offer significant advantages over conventional systems such as continuous stirred tank reactors (CSTRs) (Qin et al., 2025), including enhanced methane yield and reduced sludge production, owing to complete biomass retention and

extended solids retention time (Kwon et al., 2023; Zhu et al., 2025). For instance, Guo et al. (2022) reported a methane yield of 222.6 mL/g-VS using AnMBRs, representing a 64.0 % increase over CSTR performance under similar hydraulic retention time (HRT) conditions (Wu et al., 2020). Thus, the application of AnMBRs for SewS treatment is a promising biotechnology for resource utilization.

Membrane fouling remains a principal bottleneck hindering the widespread application of AnMBRs (You et al., 2025), particularly under high-solid anaerobic digestion conditions (Liu et al., 2023; Wu et al., 2025). Elevated levels of membrane fouling increase filtration resistance and transmembrane pressure (TMP) (Chen et al., 2025), thereby reducing sustainable membrane flux and substantially elevating the energy input required for system operation (Zhang et al., 2021). These challenges become more severe in high-solid environments (mixed

\* Corresponding author.

E-mail address: [yu.qin.e8@tohoku.ac.jp](mailto:yu.qin.e8@tohoku.ac.jp) (Y. Qin).

liquor total solids (MLTS)>30 g/L), where increased viscosity, particle concentration, and colloidal interactions exacerbate fouling dynamics and reduce the efficacy of conventional physical cleaning methods such as biogas sparging (Guo et al., 2023). Despite growing interest in fouling mitigation, most existing studies have been conducted under low to moderate solid concentrations (MLTS<30 g/L) (Gautam et al., 2022), and very few have systematically examined membrane fouling behavior in super-high solid anaerobic systems (Fan et al., 2025; Liang et al., 2025). This gap is significant, as operating under such conditions poses fundamentally different physical and biochemical challenges for membrane filtration that cannot be extrapolated from low-solid systems.

Various strategies are employed to mitigate membrane fouling, including (1) optimizing filtration cycles (Cheng et al., 2020a), (2) adding biological carriers (Lei et al., 2019), and (3) developing innovative AnMBR systems (Wang et al., 2023a,b). Unlike material-based or design-intensive interventions, filtration cycles adjustments require no physical modification to the reactor or the addition of external agents; they can be implemented through simple programmable control, making them highly applicable to both pilot and full-scale systems (Jiang et al., 2023). Despite demonstrated benefits in extending membrane longevity and sustaining flux, existing studies have several limitations that constrain their applicability to high-solid anaerobic systems (Habib et al., 2017; Park et al., 2023). First, most prior investigations have been conducted under low to moderate solid concentrations (MLTS<30 g/L), which do not fully reflect the operational realities of sludge digestion processes where solids exceed 30 g/L (Maqbool et al., 2014). Second, mechanistic understanding of fouling dynamics under high-solid conditions remains limited. Prior work has predominantly focused on aggregate indicators such as TMP or flux trends, and has employed simplified linear or exponential models to describe fouling development (Guo et al., 2023; Rong et al., 2022). Such models fall short in capturing the nonlinear, time-dependent nature of membrane fouling under constant-flux operation—a common feature of high-solid AnMBRs (Meng et al., 2009). To address these limitations, this study focuses on the dynamic evolution of TMP-flux behavior under high-solid conditions. A power-law model is applied to capture the time-dependent characteristics of membrane fouling, providing a more accurate reflection of resistance development. This modeling approach enhances process predictability and offers practical insights for improving the long-term stability of high-solid AnMBRs.

In this study, a 15 L high-solid AnMBR was employed to treat SewS. The primary objectives were to: (1) evaluate the methanogenesis of sewage sludge treated by the high-solid AnMBR in terms of COD removal, methane yield, and mass flow; (2) investigate the effects of different filtration cycles on membrane filtration, membrane fouling types and dynamics; and (3) explore the potential relationship between flux and TMP. The findings from this study will contribute to a deeper understanding of the role of filtration cycle strategies in mitigating membrane fouling, enhancing the engineering feasibility of AnMBR systems, and promoting the efficient and sustainable resource recovery of high-strength organic waste and wastewater.

## 2. Material and methods

### 2.1. Feedstock and AnMBR configuration

In this study, sewage sludge (a mixture of PS and WAS) was used as the feedstock for AD. PS and WAS were collected monthly from a WWTP in Miyagi, Japan to ensure freshness. The PS and WAS were mixed in a 50:50 ratio, approximately matching the typical yield of the WWTP, and sieved through a 1.6 mm diameter mesh to remove large debris. The prepared SewS was then added to a CSTR maintained at a constant temperature of 4 °C to ensure feedstock stability. The characteristics of the SewS are shown in Table 1.

The AnMBR consisted of a 13 L CSTR tank and a 2 L membrane tank. The CSTR was stirred at 80 rpm by an impeller to ensure complete mixing. A commercial hollow fiber membrane module made of polytetrafluoroethylene (PTFE) was used (Sumitomo Electric, Japan). The membrane had an average pore size of 0.1 μm and an effective filtration area of 0.1 m<sup>2</sup>. The sludge in the CSTR was pumped into the membrane tank via a peristaltic pump, operating at a fixed speed of 15 rpm. The sludge then flowed back into the CSTR by gravity, forming a sludge loop. The temperature of the AnMBR was maintained at 37 ± 1 °C using a water bath. The AnMBR system was operated in continuous mode. Substrate was fed five times per day using a timer-controlled peristaltic pump, with each feeding cycle lasting 90 s, resulting in a total daily influent volume of 1000 mL. To ensure mass balance between influent and effluent, 500 mL of permeate was withdrawn through membrane filtration and 500 mL of digestate was manually discharged each day. A 500 mL bottle was placed to collect the condensed water generated by cooling the air pump aeration biogas (37 ± 1 °C). The permeate and sludge discharge rates were both 500 mL/d. The HRT and SRT of the AnMBR were controlled at 15 days and 30 days, respectively, while the OLR was 3.02 ± 0.20 g-COD/L/d.

An air pump (Iwaki, APN-085LV-1, Japan) was used to flush the membrane surface with biogas sparging at a rate of 5 L/min to mitigate the rapid formation of membrane fouling. The specific gas demand per unit membrane was 3 m<sup>3</sup>/m<sup>2</sup>/h to maintain stable membrane operation. The hollow fiber membrane was equipped with a membrane fouling monitoring system, which measured TMP. This system consisted of a sensor head (Keyence, AP-10S, Japan), a data display module (Keyence, AP-V85, Japan), and a multi-unit compatible data acquisition system (Keyence, NR-5000, Japan).

The sludge concentration in the reactor was adjusted to maintain a MLTS concentration of 30–35 g/L by formula (1), thereby eliminating the influence of changes in sludge concentration and characteristics on the experiment:

$$V_{\text{per}} = V_{\text{reactor}} \left( \frac{C_0}{C_{\text{target}}} - 1 \right) \quad (1)$$

In which  $C_0$  is the initial MLTS of the AnMBR,  $C_{\text{target}}$  is the target MLTS of the reactor,  $V_{\text{reactor}}$  is the working volume of the AnMBR, and  $V_{\text{per}}$  is the volume of discharged permeate.

**Table 1**  
Characteristics of sewage sludge.

Item	Unit	Value	Item	Unit	Value	Item	Unit	Value
TS	g/L	32.93 ± 0.89	VS	g/L	27.02 ± 0.89	FS	g/L	5.89 ± 0.26
TSS	g/L	28.34 ± 0.68	VSS	g/L	21.04 ± 0.13	FSS	g/L	7.30 ± 0.78
T-COD	g/L	44.13 ± 3.73	Sup-COD	g/L	6.48 ± 1.75	S-COD	g/L	4.77 ± 0.52
T-car	g/L	13.16 ± 3.52	Sup-car	g/L	0.41 ± 0.09	S-car	g/L	0.39 ± 0.10
T-pro	g/L	13.54 ± 1.07	Sup-pro	g/L	1.24 ± 0.49	S-pro	g/L	0.70 ± 0.10
pH	/	5.54 ± 0.13	VFAs	g/L	1.84 ± 0.56	NH <sub>4</sub> <sup>+</sup> -N	mg/L	318 ± 108
Lipid	g/L	0.12 ± 0.02						

T-COD: Total COD, Sup-COD: Supernatant COD, S-COD: Soluble COD, T-car: Total carbohydrate, Sup-car: Supernatant carbohydrate, S-car: Soluble carbohydrate, T-pro: total protein, Sup-pro: supernatant protein, S-pro: Soluble protein. FS: Fixed solids. FSS: Fixed suspended solids.

## 2.2. Chemical analysis

Biogas production in the reactor was measured using a wet gas flow meter and converted into biogas production under standard conditions using the ideal gas law. The concentrations of CH<sub>4</sub> and CO<sub>2</sub> in the biogas were measured daily using a gas chromatograph (Shimadzu GC-8A) equipped with a Porapak Q-packed column and a thermal conductivity detector. For each analysis, 0.4 mL of gas was manually injected. Calibration was performed using high-purity CH<sub>4</sub> and CO<sub>2</sub> standard gases (purity ≥99.99 %) at injection volumes of 0.1, 0.2, 0.3, and 0.4 mL to establish standard curves. Feedstock, AnMBR sludge, and permeate samples were collected every Wednesday and Saturday, then centrifuged at 15,000 rpm for 15 min to obtain the supernatant, which was subsequently filtered through a 0.45 µm filter membrane to obtain the filtrate. The relevant properties of the original sample, supernatant, and filtrate were tested and analyzed. Total solids (TS), volatile solids (VS), total suspended solids (TSS), and volatile suspended solids (VSS) were determined using gravimetric analysis (Song et al., 2024). Chemical oxygen demand (COD), carbohydrates, and proteins were quantified using standard methods described in a previous report (Qin et al., 2024). Alkalinity was measured by titration with 0.1 mol/L HCl, with bicarbonate and total alkalinity determined based on pH endpoints of 6.5 and 4.8, respectively. VFAs were analyzed using a gas chromatograph (Agilent 6980N) equipped with a DB-WAX<sub>etr</sub> capillary column and a flame ionization detector. The viscosity of AnMBR sludge, maintained at a constant temperature of approximately 37 ± 1 °C in a water bath, was measured using a viscometer (ASJ-8ST).

## 2.3. Methods for membrane performance analysis

### 2.3.1. Membrane fouling analysis theory

The rate of change in TMP over time serves as a valuable indicator of the primary membrane fouling mechanisms: pore blocking and cake layer development (Sreedhar et al., 2022). A constant TMP overtime suggests that slight pore blocking is the dominant mechanism, whereas a steady increase in TMP indicates the dominance of the rough cake layer mechanism (Fig. S1). A sharp increase in TMP signifies the formation of a dense cake layer.

### 2.3.2. Membrane fouling type

Identifying membrane fouling types is essential for optimizing filtration performance and prolonging membrane lifespan, and in this study, the pore clogging filtration model was applied for fouling identification, as shown in formula (2) (Hermia, 1982).

$$\frac{dp}{dv} = k' p^{n'} \quad (2)$$

Where  $p$  represents the filtration pressure (Pa);  $k'$  is the clogging coefficient, with units of kg<sup>1-n'</sup>·m<sup>n'-2</sup>·s<sup>2n'-2</sup>; and  $n'$  is the exponent. Where  $n' = 2.0$ , the filtration mechanism corresponds to complete pore blocking. Where  $n' = 1.5$ , the filtration follows the standard pore-blocking model. Where  $n' = 1.0$ , the filtration process is characterized by intermediate pore blocking. Conversely, where  $n' = 0$ , the process represents cake filtration.

## 2.4. Different filtration cycles settings

The experimental configurations for the nine filtration cycle groups are presented in Table 2. Each filtration cycle lasted 4 h, during which TMP was continuously monitored. The instantaneous flux ( $J_0$ ) was measured at 30-min intervals to track fouling dynamics.

Two sets of experimental conditions were employed: In the first set (upper portion of Table 2), the F/R was fixed at 1.0, while the individual filtration and relaxation times varied from 0.75 to 3 min. In the second set (lower portion of Table 2), the total cycle time was fixed at 4 min,

**Table 2**  
Different filtration cycles in the AnMBR.

	$J_0$ (LMH)	Filtration: Relaxation	F/R	$\bar{J}$ (LMH)
Same filtration/relaxation ratio				
I	11.88 ± 0.04	0.75 min: 0.75 min	0.75:0.75 = 1.00	5.94 ± 0.02
II	11.79 ± 0.03	1 min: 1 min	1:1 = 1.00	5.87 ± 0.04
III	11.57 ± 0.02	2 min: 2 min	2:2 = 1.00	5.78 ± 0.01
IV	11.52 ± 0.06	3 min: 3 min	3:3 = 1.00	5.79 ± 0.10
Different filtration/relaxation ratios				
I	20.10 ± 0.60 ( $J^*$ = 23.60)	1 min: 3 min	1:3 = 0.33	5.03 ± 0.15
II	16.68 ± 0.06 ( $J^*$ = 17.70)	1 min: 2 min	1:2 = 0.50	5.60 ± 0.02
III	11.79 ± 0.03	1 min: 1 min	1:1 = 1.00	5.89 ± 0.04
IV	8.96 ± 0.01	2 min: 1 min	2:1 = 2.00	5.97 ± 0.01
V	8.02 ± 0.04	3 min: 1 min	3:1 = 3.00	6.02 ± 0.03
VI	7.42 ± 0.01	4 min: 1 min	4:1 = 4.00	5.92 ± 0.03

$J_0$  refers to the actual instantaneous flux.  $\bar{J}$  refers to the average flux.  $J^*$  refers to the membrane instantaneous flux expected to achieve.

while the F/R varied from 1:3 to 4:1 by adjusting the duration of filtration and relaxation.

To enable fair comparisons across filtration cycles, the average membrane flux ( $\bar{J}$ ) was consistently maintained at approximately 5.9 LMH in all experiments, which falls between the critical flux ( $J_c = 4.12$  LMH) and threshold flux ( $J_t = 6.63$  LMH), determined via the flux-stepping experiment (Fig. S2). The required theoretical  $J_0$  values for each F/R were calculated accordingly and are provided in brackets in Table 2.

After each 4-h filtration cycle, the membrane underwent biogas sparging for at least 24 h to ensure full restoration of membrane performance before the next set experiment cycle. The baseline performance for all filtration cycles is shown in Fig. S3 and Fig. S4. Irreversible fouling that was not removed by biogas sparging was assessed at the conclusion of all experiments, with flux membrane recovery for the 1:1 cycle decreasing from 76.1 % to 72.6 % (a flux loss of over 3.5 %) as shown in Fig. S5, which remains within the 5 % margin of error, ensuring data reliability.

## 2.5. Calculations

To assess the performance of the AnMBR system in treating organic matter, the removal efficiency of COD was calculated (Ye et al., 2023).

$$R (\%) = \frac{C_{\text{sewage sludge}} - C_{\text{permeate}}}{C_{\text{sewage sludge}}} \times 100 \quad (3)$$

Where  $C_{\text{sewage sludge}}$  and  $C_{\text{permeate}}$  is the concentration of total COD in SewS and permeate, respectively.

The calculation of average flux is shown in formula (4):

$$\bar{J} = J_0 \cdot D \quad (4)$$

where  $\bar{J}$  refers to the average flux,  $J_0$  refers to the actual instantaneous flux,  $D$  is the duty ratio, commonly defined as the ratio of the on-time (i.e., power-on or operating time) to the total duration of one complete cycle, which includes both operating and non-operating time. The duty ratio is calculated using formula (5):

$$D = \frac{F}{F+R} = \frac{F/R}{(F/R)+1} \quad (5)$$

where  $F$  is the filtration time and  $R$  is the relaxation time.

The flux maintenance efficiency (FME) was calculated using formula (6) to ensure fair comparison between groups by accounting for potential errors in the average flux:

$$\text{Flux maintenance efficiency (\%)} = \frac{J_{240 \text{ min}}}{J_0 \text{ min}} \times 100\% \quad (6)$$

where  $J_0 \text{ min}$  is the instantaneous flux measured when the membrane has been running for 0 min (LMH), and  $J_{240 \text{ min}}$  is the instantaneous flux measured after 240 min of operation (LMH).

The filtration resistance for the cake layer was investigated using the resistance-in-series theory (Niu et al., 2020). The total resistance ( $R_T$ ) was calculated using formula (7) to further quantify membrane fouling:

$$R_T = \frac{\text{TMP}}{\mu J} \quad (7)$$

where  $\mu$  is the viscosity of AnMBR sludge (Pa·s), and  $J$  is the flux (LMH).

### 3. Results and discussion

#### 3.1. Long-term methanogenic performance & mass balance

Data were recorded once the biogas production rate and methane composition of the AnMBR had stabilized. The methanogenic performance of the AnMBR was monitored by measuring the MLTS, pH, biogas production rate, and biogas composition, as shown in Fig. 1. The MLTS was high, at  $33.7 \pm 1.0 \text{ g/L}$ , due to the concentrating effect of the membrane. A linear relationship between operation time and MLTS indicated a decrease in MLTS over time, with a rate of approximately  $0.0018 \text{ g/L per day}$ . The biogas production rate of the AnMBR was  $0.74 \pm 0.07 \text{ L/L/d}$ . The  $\text{CH}_4$  content was  $62.3 \pm 0.8 \%$ , and the  $\text{CO}_2$  content was  $35.1 \pm 0.9 \%$ . The calculated methane yield was  $157.8 \pm 15.3 \text{ mL-CH}_4/\text{g-COD}_{\text{add}}$  and  $258.5 \pm 24.0 \text{ mL-CH}_4/\text{g-VS}_{\text{add}}$ . The methane yield was 26.7 % higher than that observed in the AD of WAS after microwave pretreatment, which had a methane yield of  $204.1 \pm 18.1 \text{ mL-CH}_4/\text{g-VS}_{\text{add}}$  (Liu et al., 2020). The efficient methanogenic performance of the AnMBR was facilitated by the membrane's rejection of microorganisms (Cheng et al., 2024). To evaluate the extent of substrate conversion and validate the accuracy of the data, the methane yield was compared with theoretical upper limits. Based on the improved Buswell equation, the theoretical methane yield for SewS typically ranges between 350 and 400  $\text{mL-CH}_4/\text{g-VS}_{\text{add}}$  (depending on sludge composition and biodegradability) (Raposo et al., 2012). The observed methane yield in this

study accounted for approximately 65–74 % of the theoretical maximum, which is reasonable considering the complexity and partial degradability of SewS. The AnMBR achieved highly efficient pollutant removal. Specifically, the permeate COD concentration ranged from 294.0 to 455.8 mg/L, with an average of 384.3 mg/L, and the COD removal efficiency remained stable at  $99.1 \pm 0.1 \%$ .

As shown in Fig. 1, the operational stability of the AnMBR was confirmed by continuous monitoring of pH and total-alkalinity. Throughout the run, the pH remained at  $7.22 \pm 0.08$ , total-alkalinity at  $3.6 \pm 0.3 \text{ g/L}$  and VFAs at  $15.4 \pm 11.6 \text{ mg/L}$ . The sufficient microbial biomass in the reactor ensured efficient degradation of organic matter (Liu et al., 2024). On one hand, the VFAs produced during the acidogenesis and acetogenesis stages were promptly utilized by methanogens. On the other hand, the protein degradation efficiency of  $55.9 \pm 3.9 \%$  led to the release of a large amount of ammonia nitrogen, reaching  $1221 \pm 89 \text{ mg/L}$  (Fig. S6). Together, the low VFA concentration and high alkalinity maintained a robust anaerobic system. To further evaluate system performance and element retention behavior, the mass balance of  $\text{NH}_4^+$ -N and TP during the treatment of 1 ton sewage sludge via the AnMBR system is illustrated in Fig. S7.

The mass flow for SewS treatment in the AnMBR is shown in Fig. 2, in which  $\text{CH}_4$ , carbohydrates, proteins, and lipids are all expressed in terms of COD, based on specific conversion coefficients (Li et al., 2024). When the feed was SewS, protein was the main component, accounting for 46.17 %. Of the COD in the feed, 46.78 % was converted into methane bioenergy through AnMBR treatment, while only 0.54 % of the COD was lost in the permeate, demonstrating the excellent performance of the AnMBR system. Specifically, 6.74 g-COD/L of readily degradable carbohydrates was converted to methane. In contrast, only 7.74 g-COD/L of protein (representing just 38.13 % of protein-COD in the feed) was transformed into methane, while a greater portion—approximately 54.60 %—was discharged with the digestate or remained in the permeate. Additionally, 0.24 g-COD/L of lipids was biodegraded and converted into methane.

#### 3.2. Membrane filtration performance

##### 3.2.1. Identical filtration/relaxation ratio

The effects of filtration and relaxation spans on membrane filtration

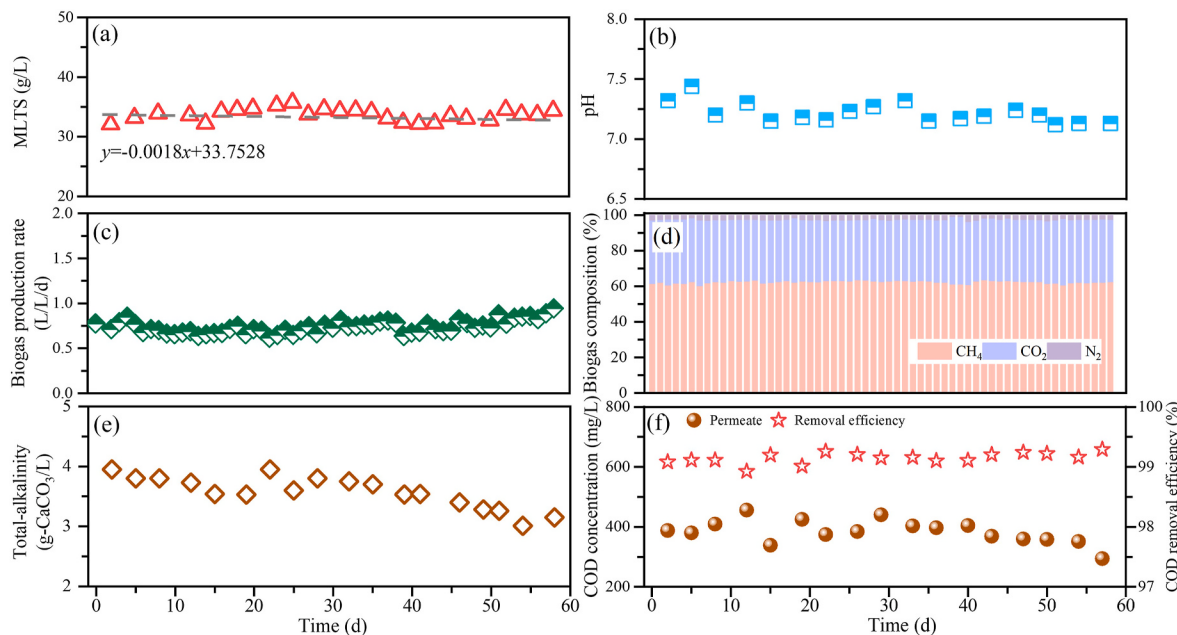
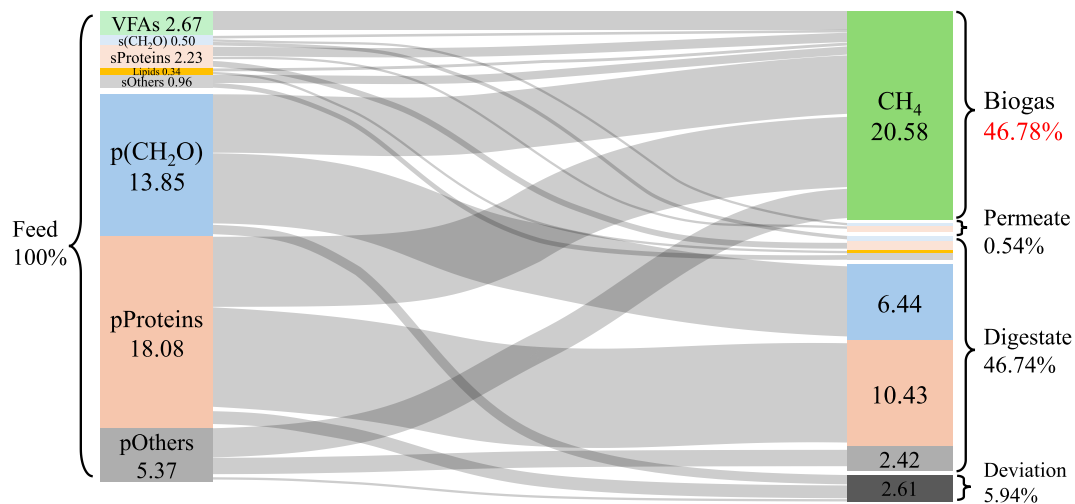


Fig. 1. High-solid AnMBR long-term performance: MLTS (a), pH (b), biogas production rate (c), biogas composition (d), total-alkalinity (e), Permeate COD concentration and COD removal efficiency (f).



**Fig. 2.** Mass flow for the treatment of sewage sludge in the AnMBR (unit: g-COD/L) (g). The prefixes "s" and "p" before the title indicate the distribution of organic matter in the "supernatant" and "particulates," respectively. (CH<sub>2</sub>O) represents carbohydrates.

performance with a constant F/R of 1 are shown in Fig. 3. Filtration time had a notable effect on Max-TMP, with Max-TMP increasing from 44.85 ± 0.06, 44.91 ± 0.01, 47.71 ± 0.12 to 51.01 ± 0.21 kPa as the filtration time was extended from 0.75, 1, 2 to 3 min, respectively. A longer relaxation time, coupled with extended concentration polarization and biogas sparging, was more effective in removing the cake layer from the membrane surface, thus alleviating membrane fouling. Consequently, Min-TMP decreased from 23.11 ± 0.21, 14.77 ± 0.49, 7.28 ± 0.16 to 2.15 ± 0.08 kPa as the relaxation time increased from 0.75, 1, 2–3 min, respectively.

The ΔTMP for the 0.75:0.75, 1:1, 2:2, and 3:3 cycles increased from 21.74 ± 0.27, 30.14 ± 0.49, 40.42 ± 0.04 to 48.86 ± 0.29 kPa, indicating that membrane fouling was mildest at the 0.75:0.75 cycle. However, contaminants may still accumulate without causing a proportional increase in TMP—particularly when forming loose and compressible fouling layers. Such fouling can reduce the effective filtration area or clog membrane pores, thereby impairing membrane performance even under relatively stable TMP conditions. This trend is reflected in the FME, which was 73.1 %, 76.1 %, 67.3 %, and 66.7 % for the 0.75:0.75, 1:1, 2:2, and 3:3 filtration cycles, respectively. These results demonstrate that the 1:1 filtration cycle offered clear advantages in filtration performance, with membrane flux improving by at least 4.1 % compared to the other cycles. This can be attributed to the fact that an overly short rest time (0.75:0.75) prevents adequate recovery of fouling on the membrane surface, negatively affecting the FME. Conversely,

extending the operation time (2:2 and 3:3) resulted in more severe membrane pore blockage, making prolonged relaxation ineffective in restoring performance. Although the F/R was 1 across all four filtration cycles, selecting an optimal filtration and relaxation time proved beneficial for enhancing membrane filtration performance. Recent research also indicates that the F/R affects pump energy consumption and, consequently, economic efficiency, with higher F/R values leading to lower energy consumption (Park et al., 2023). Therefore, achieving a balance between filtration performance and energy efficiency is another crucial factor to consider.

### 3.2.2. Different filtration/relaxation ratios

The membrane filtration performances of 1:3, 1:2, 1:1, 2:1, 3:1, and 4:1 are shown in Fig. 4. At an F/R of 1:3, the expected  $J_0$  required to achieve the target  $\bar{J}$  of 5.90 LMH was 23.60 LMH. However, the actual  $J_0$  achieved was only 20.10 ± 0.60 LMH, corresponding to a 14.83 % loss compared to the expected value. This discrepancy exceeded the commonly accepted deviation threshold of 10 %, and therefore, the 1:3 condition was excluded from further comparative analysis to ensure performance reliability. This deviation likely arose from equipment limitations, particularly the inability of the peristaltic pump to accurately deliver high preset fluxes over short filtration periods. In addition, the high  $J_0$  may have caused rapid membrane fouling, leading to an early rise in ΔTMP (>30 kPa), which exceeded the normal operational range and indicated system instability. This pressure exceeded the

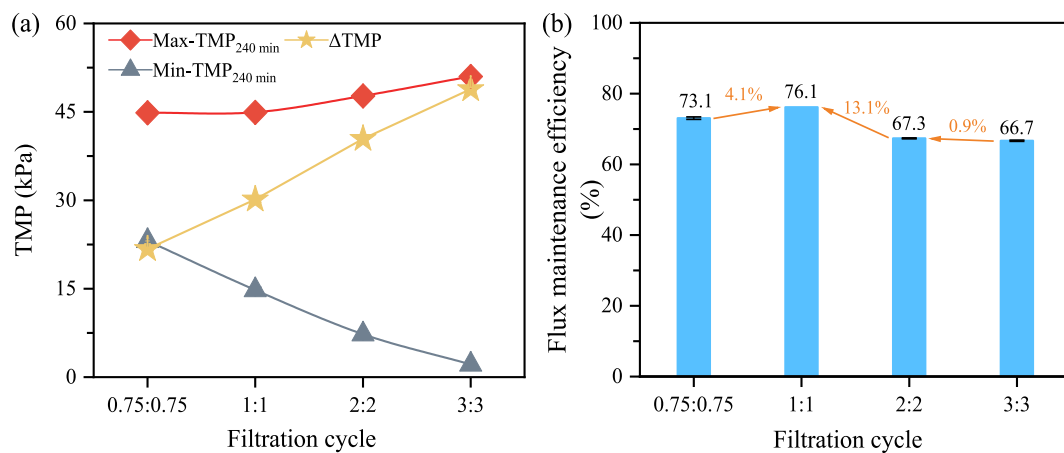


**Fig. 3.** Membrane filtration performance under constant instantaneous flux and F/R: TMP (a) and Flux maintenance efficiency (b).

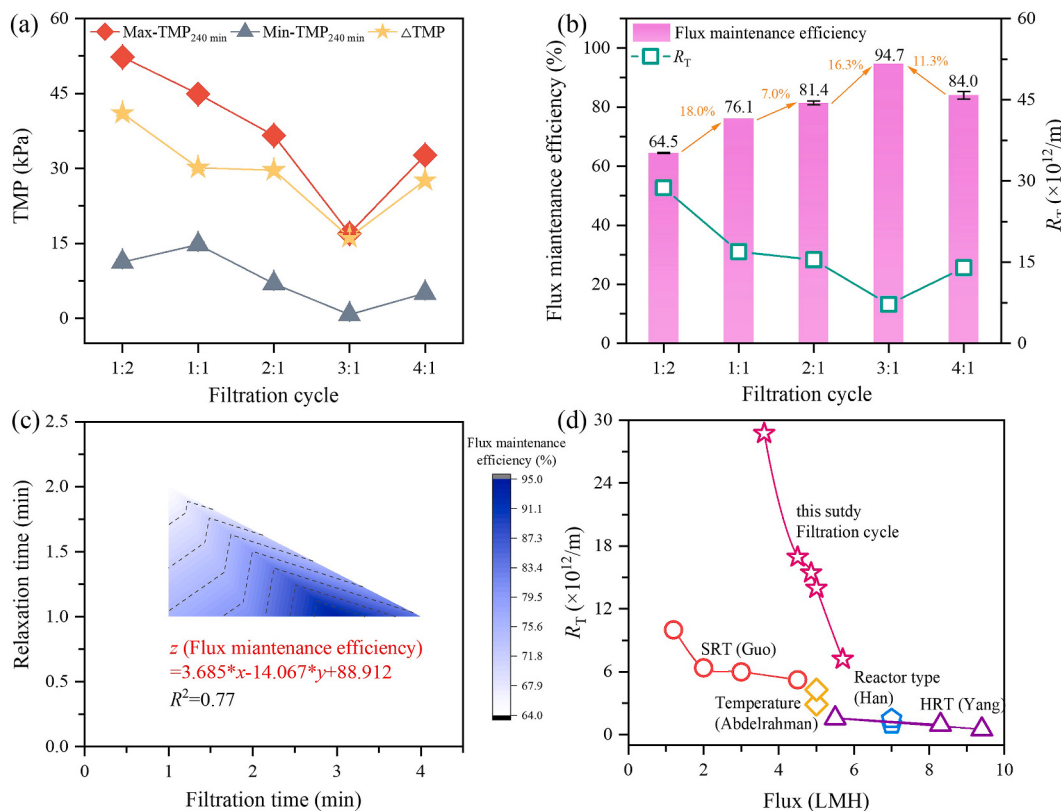


**Fig. 4.** Membrane filtration performance under different instantaneous flux and F/R: TMP (a), Flux maintenance efficiency and  $R_T$  (b). The relationship between filtration time, relaxation time and flux maintenance efficiency (c). Comparison of Flux and  $R_T$  with previous studies (d).

normal operational range for microfiltration systems—typically maintained below 30–40 kPa due to their negative-pressure operation—and indicated the onset of system instability (Wang et al., 2023a,b).

As the F/R increased from 1:2, 1:1, 2:1 to 3:1,  $\Delta\text{TMP}$  decreased from  $41.02 \pm 0.51$ ,  $30.14 \pm 0.49$ ,  $29.66 \pm 0.15$  to  $16.23 \pm 0.05$  kPa, respectively, and the corresponding FME increased from 64.5 % to 76.1 %, 81.4 %, and 94.7 %. When the F/R further increased from 3:1 to 4:1,  $\Delta\text{TMP}$  increased from  $16.23 \pm 0.05$  to  $27.61 \pm 0.03$  kPa, and FME decreased from 94.7 % to 84.0 %, indicating that the 3:1 filtration cycle exhibited the best filtration performance. The development of membrane fouling could be effectively controlled at the 3:1 filtration cycle. The Max-TMP<sub>240 min</sub> and Min-TMP<sub>240 min</sub> were both at their minimum values,  $17.00 \pm 0.16$  kPa and  $0.77 \pm 0.11$  kPa, respectively. The  $R_T$  remained at the minimum value of  $7.20 \times 10^{12} \text{ m}^{-1}$ . The membrane flux was effectively improved by at least 11.3 % compared with other filtration cycles. These results show that optimizing the filtration cycle can effectively alleviate membrane fouling and stabilize membrane flux. The relationship between filtration time, relaxation time, and FME was further analyzed, and the relationship is described by the equation:  $z = 0.8891 + 0.0369x - 0.1407y$ , as shown in Fig. 4 (c). This equation provides quantitative guidance for optimizing FME and offers a way to effectively enhance membrane filtration performance by adjusting filtration and relaxation times.

The flux and  $R_T$  variations under different experimental conditions in AnMBR are shown in Fig. 4 (d). Factors such as hydraulic retention time (ranging from 5.5 to 9.4 h) (Yang et al., 2024), temperature (mesophilic vs. thermophilic conditions) (Zhang et al., 2025), and reactor type (transition from AnMBR to electrochemical AnMBR) demonstrated some anti-fouling capabilities (Jeison and van Lier, 2006). When the SRT was reduced from 60 days to 30 days, membrane flux increased by 3.75 times, and filtration resistance decreased by 47.7 % (Guo et al., 2023). Moreover, the filtration cycle exhibited a significant reduction in filtration resistance, underscoring its distinct advantages in mitigating

membrane fouling and effectively controlling resistance.

### 3.3. Quantitative analysis between filtrate volume and $\Delta\text{TMP}$

To further investigate the relationship between cumulative filtrate volume and  $\Delta\text{TMP}$  during each filtration cycle, the experimental data were analyzed and were shown in Fig. 5. The results revealed a distinctly nonlinear relationship between  $\Delta\text{TMP}$  and cumulative flux, which was accurately described by a power-law function, as given by equations (8) and (9):

$$\ln(\Delta\text{TMP}) = k \cdot \ln(v) + b \quad (8)$$

$$\Delta\text{TMP} = e^b v^k \quad (9)$$

Here,  $v$  represented the cumulative flux ( $\Sigma J$ ),  $k$  is the power-law exponent representing the rate of fouling progression, and  $b$  is the intercept reflecting the initial pressure resistance—largely influenced by pump pressure and baseline membrane resistance. This formulation aligns with the mechanistic understanding of fouling behavior: as filtration proceeds, the accumulation and compression of cake-layer materials often result in an accelerated rise in  $\Delta\text{TMP}$ , deviating from the assumptions of linear or exponential models (An et al., 2023; Lin et al., 2013). Among the compared models, including linear, exponential, and power-law formulations, the power-law model achieved the highest average coefficients of determination ( $R^2$ ) value (0.7957), indicating superior goodness of fit (Fig. 5(i)).

The power-law model was selected for its dual advantages of empirical robustness and physical interpretability. Unlike linear or exponential expressions, which assume either constant or uniformly accelerating fouling rates, the power-law formulation better captures the nonlinear, time-dependent evolution of fouling, particularly under constant-flux and cyclic operation modes typical of high-solid AnMBRs.

The high  $R^2$  observed across all tested filtration cycles confirm the

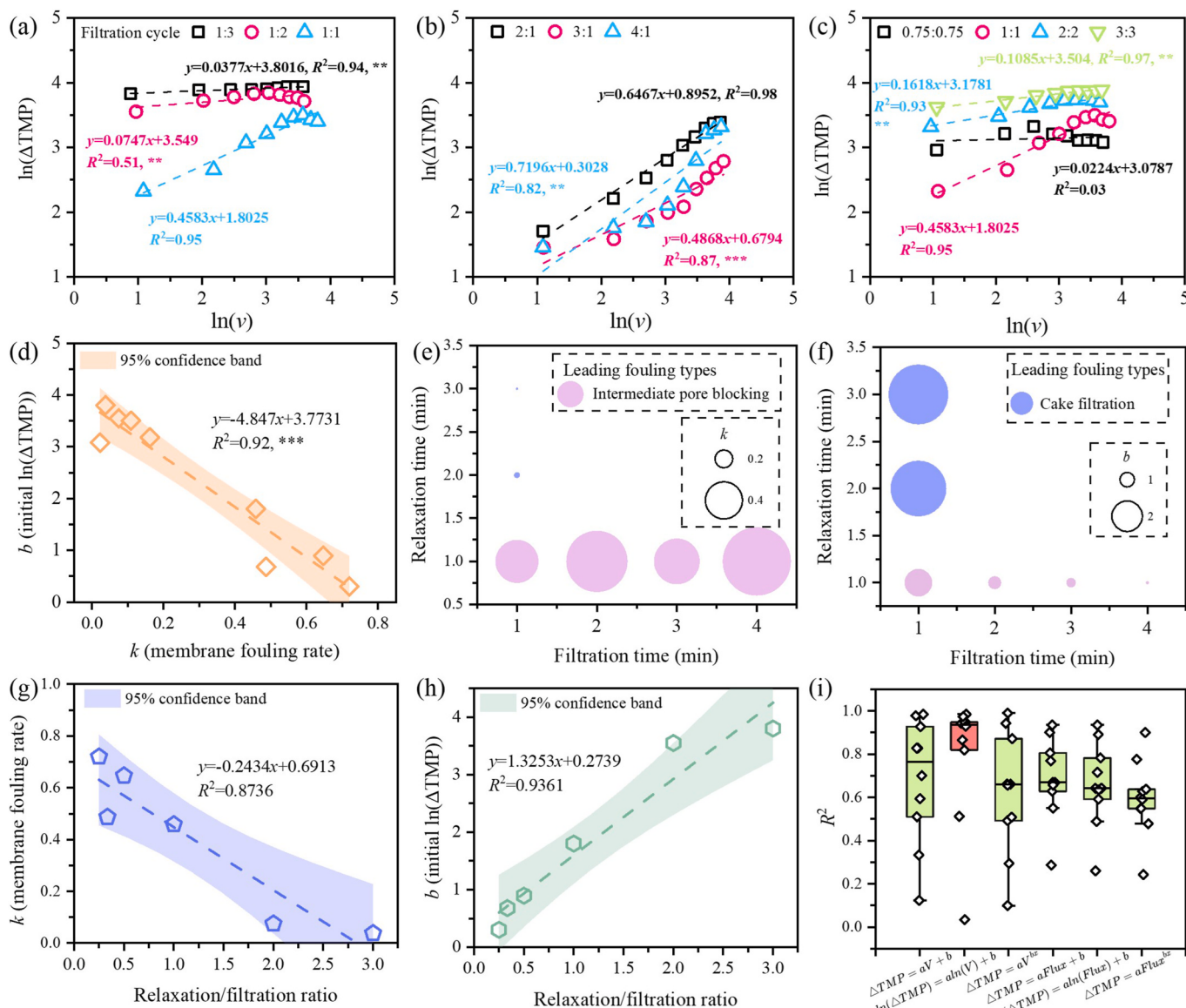


**Fig. 5.** The linear relationship between  $\ln(v)$  and  $\ln(\Delta\text{TMP})$  for different filtration cycles (a), (b) and (c). Significant differences among phases were determined using independent-sample t-test: \* $p < 0.05$ , \*\* $p < 0.01$ , and \*\*\* $p < 0.001$ . The linear relationship between  $k$  (membrane fouling rate) and  $b$  (initial  $\ln(\Delta\text{TMP})$ ) (d). Effects of filtration time and relaxation time on  $k$  and  $b$  (e), (f), where  $k$  and  $b$  represent the slope and intercept of the linear relationship between  $\ln(v)$  and  $\ln(\Delta\text{TMP})$ , respectively. The linear relationship between the Relaxation/Filtration ratio and  $k$  (g), and  $b$  (h).  $R^2$  comparison of different  $\Delta\text{TMP}$  modeling approaches (i).

statistical validity of this model. Moreover, the parameters  $k$  and  $b$  offer quantitative indicators of fouling behavior that can be used for real-time performance monitoring or adaptive control—making this model not only descriptive but also predictively valuable and scalable for engineering applications.

As shown in Fig. 5(a), filtration cycles with longer relaxation periods (e.g., 1:3 and 1:2) exhibited higher initial  $\Delta\text{TMP}$  but much slower fouling rates, with  $k$  values of 0.037 and 0.0747. This suggests that although the higher  $J_0$  in these cycles initially increased  $b$ , the extended relaxation effectively removed loosely attached foulants and mitigated cake buildup, thus keeping  $k$  low. In contrast, shorter relaxation cycles (e.g., 2:1, 3:1, 4:1) showed lower initial  $\Delta\text{TMP}$ s (i.e., lower  $b$ ), but much steeper increases in TMP over time, with  $k$  values reaching 0.6467, 0.4868, and 0.7196, respectively (Fig. 5(b)). This indicates that insufficient relaxation led to poor fouling control and accelerated resistance accumulation. As illustrated in Fig. 5(f), a negative linear correlation between  $k$  and  $b$  further supports that aggressive relaxation schemes can suppress fouling propagation even if initial resistance is high. These

findings suggest that  $k$  can serve as a dynamic indicator of fouling progression, while  $b$  reflects the system's initial filtration resistance under a given F/R. Monitoring changes in these parameters enables early identification of fouling trends and offers a rational basis for optimizing filtration cycles in engineering practice. Moreover, based on the calculations, the overall relationship between  $\ln(\Delta\text{TMP})$  and  $\ln(v)$  under different filtration cycles followed the equation:  $\ln(\Delta\text{TMP}) = 0.3018\ln(v)+2.3101$ .

The relationship between F/R and  $k$  (membrane fouling rate) as well as  $b$  (initial  $\ln(\Delta\text{TMP})$ ) is illustrated in Fig. 5. The  $R^2$  values for the linear fits,  $y=-0.2434x+0.6913$  and  $y=1.3253x+0.2739$  are 0.8736 and 0.9361, respectively, indicating strong fit performance that effectively describes the relationship between the Relaxation/Filtration ratio (the inverse of the Filtration/Relaxation ratio) and both  $k$  and  $b$ . In Fig. 5(g), the data shows that the membrane fouling rate,  $k$ , decreases significantly as the relaxation time increases. Conversely, Fig. 5(h) demonstrates that as the relaxation time decreases, the initial  $\Delta\text{TMP}$  increases. These findings underscore the critical balance between filtration time and

relaxation time and their combined impact on performance.

### 3.4. Membrane fouling dynamics

The membrane fouling mathematical model and real-time TMP curves are integrated to analyze both the type and severity of membrane fouling. The leading fouling types for each filtration cycle are presented in Table 3. When filtration and relaxation times were equal (e.g., 1:1, 2:2, 3:3), fouling was predominantly characterized by cake layer formation, which is relatively easy to remove. Under different F/R, filtration cycles with higher  $J_0$  (16.68–20.10 LMH) and shorter filtration times (1 min) primarily exhibited cake filtration, indicating that foulants accumulated mainly on the membrane surface. In contrast, filtration cycles with lower  $J_0$  (7.42–11.79 LMH) and longer filtration durations (1–4 min filtration time) predominantly resulted in intermediate pore blocking, suggesting that surface-deposited foulants had more time to compact and infiltrate into membrane pores (Cheng et al., 2020b). Interestingly, a 3-min filtration followed by 1-min relaxation (3:1 cycle) limited pore intrusion while still allowing sufficient back-transport during relaxation, achieving the highest FME of 94.7 %. These results highlight the critical role of filtration cycle design in balancing the removal of surface fouling and the prevention of internal pore blockage. By tailoring the filtration duration and relaxation interval, membrane resistance can be better controlled, enabling more stable and sustainable filtration performance.

The representative TMP curves under 3:1, 4:1, and 1:2 filtration cycles are chosen to analyze membrane fouling mechanisms (Fig. 6). The optimal filtration performance was achieved at the 3:1 filtration cycle. Max-TMP increased slowly at a rate of 0.056 kPa/min during the 3-min filtration. Biogas sparging and concentration polarization effectively removed pollutants from the membrane surface during the 1-min relaxation phase (Xu et al., 2020). As shown in Fig. 6 (a), the Min-TMP recovered to its initial value, indicating that the rough cake layer (reversible fouling) formed during the 3-min filtration could be completely removed in the 1-min relaxation. However, after 240 min of filtration, the FME dropped to 94.7 %, suggesting relatively slight irreversible fouling on the membrane pores. Although the minor pollutant accumulation did not significantly impact overall TMP recovery, it still reduced membrane filtration performance. More critically, the continuous accumulation of pollutants during long-term operation exacerbates membrane fouling. Therefore, chemical cleaning methods are essential for maintaining stable membrane operation.

The real-time TMP curve for the 4:1 filtration cycle is shown in Fig. 6 (b). The growth rate of Max-TMP was slow, at 0.052 kPa/min, while Min-TMP remained stable during the initial stage. After 120 min of filtration, Max-TMP increased rapidly, first at a rate of 0.245 kPa/min and later at 0.099 kPa/min, while Min-TMP increased at 0.056 kPa/min. The membrane fouling process occurred in two stages: slow and rapid fouling, consistent with previous studies (Zhang et al., 2025). When the filtration cycle was changed from 3:1 to 4:1, the  $J_0$  decreased from 8.02 to 7.42 LMH, with minimal change in the attraction of contaminants.

**Table 3**  
Leading fouling types under different filtration cycles.

Filtration: Relaxation	$n'$	$R^2$	Leading fouling types
Fixed filtration/relaxation ratio			
0.75 min: 0.75 min	0.312	0.916	Cake filtration
1 min: 1 min	0.548	0.992	Intermediate pore blocking
2 min: 2 min	0.223	0.991	Cake filtration
3 min: 3 min	0.121	0.991	Cake filtration
Different filtration/relaxation ratios			
1 min: 3 min	0.040	0.918	Cake filtration
1 min: 2 min	0.150	0.968	Cake filtration
1 min: 1 min	0.548	0.992	Intermediate pore blocking
2 min: 1 min	0.685	0.993	Intermediate pore blocking
3 min: 1 min	0.509	0.920	Intermediate pore blocking
4 min: 1 min	0.745	0.857	Intermediate pore blocking

However, extending the filtration time from 3 to 4 min (a 33 % increase) resulted in tighter binding of contaminants to the membrane surface and pores. The minor pollutants that accumulated during the slow TMP growth stage contributed to the development of membrane fouling over long-term operation, causing a faster increase in TMP. Compared to the 3:1 filtration cycle, longer filtration time led to a greater accumulation of foulants within the membrane pores, resulting in severe pore blocking that could not be removed by the biogas sparging. This caused more severe membrane fouling, resulting in an FME of only 84.0 %.

The real-time TMP curve for the 1:2 filtration cycle is shown in Fig. 6 (c). The  $J_0$  increased sharply from 8.02 to  $16.68 \pm 0.06$  LMH, enhancing the suction force on pollutants and leading to varying fouling behaviors. This caused a rapid, logarithmic increase in the Max-TMP during the initial stage, while the Min-TMP rose at a rate of 0.055 kPa/min. The increased suction force on pollutants contributed to the formation of a dense cake layer (Jeison and van Lier, 2006). Previous studies have shown that surpassing the critical flux is more likely to result in irreversible fouling (Hu et al., 2021). The increased suction force caused more pollutants to block membrane pores and accumulate on the membrane surface, raising filtration resistance and reducing the FME to only 64.5 %. Even with the relaxation time extended to 2 min, it was still impossible to remove all contaminants from the membrane surface. Therefore, maintaining appropriate F/R ratios and  $J_0$  is crucial for the long-term stable operation of the membrane.

### 3.5. Prospects and outlook

#### 3.5.1. Prospects for practical application

The findings of this study demonstrate that F/R optimization offers a practical and effective approach to mitigating membrane fouling in high-solid AnMBRs. Among the nine F/R tested, the 3:1 cycle achieved the best trade-off between maintaining filtrate productivity and controlling membrane fouling. The empirical power-law model further allowed for a straightforward yet effective interpretation of fouling progression, providing a useful predictive framework for process evaluation.

One key advantage of this strategy lies in its high implementation feasibility. Unlike chemical cleaning, physical backflushing, or structural retrofitting, the proposed filtration cycles can be easily executed through programmable timer-controlled pumps. This control-based strategy requires no additional infrastructure or materials, making it highly suitable for both retrofitting and scale-up in existing AnMBR installations (Zhu et al., 2025). The current approach aligns with a Technology Readiness Level of 5–6 (i.e., validated in lab conditions with scalable potential), and further pilot-scale demonstration is warranted to advance toward full-scale deployment.

While the 3:1 filtration cycle showed optimal performance under laboratory conditions, its application at full scale may introduce certain trade-offs. Extended relaxation periods could reduce net filtration time and require precise timer control, increasing system complexity. If biogas sparging is used during relaxation, energy consumption may also rise. To address these challenges, future work should evaluate energy–productivity trade-offs and explore adaptive control strategies that adjust filtration cycles based on real-time fouling indicators (e.g.,  $\Delta$ TMP slope). These efforts will help ensure the proposed approach remains both technically and economically viable at full scale.

#### 3.5.2. Limitations and future research directions

While the proposed filtration cycles adjustments strategy and modeling framework show strong potential for practical application, there remain several limitations that merit further investigation to enhance their robustness and scalability. (1) Limited granularity of filtration time intervals: The present study investigated discrete filtration durations (0.75, 1, 2, and 3 min), which may overlook transitional behaviors. Future studies could employ finer time resolutions to more precisely define optimal conditions. (2) Absence of mechanistic

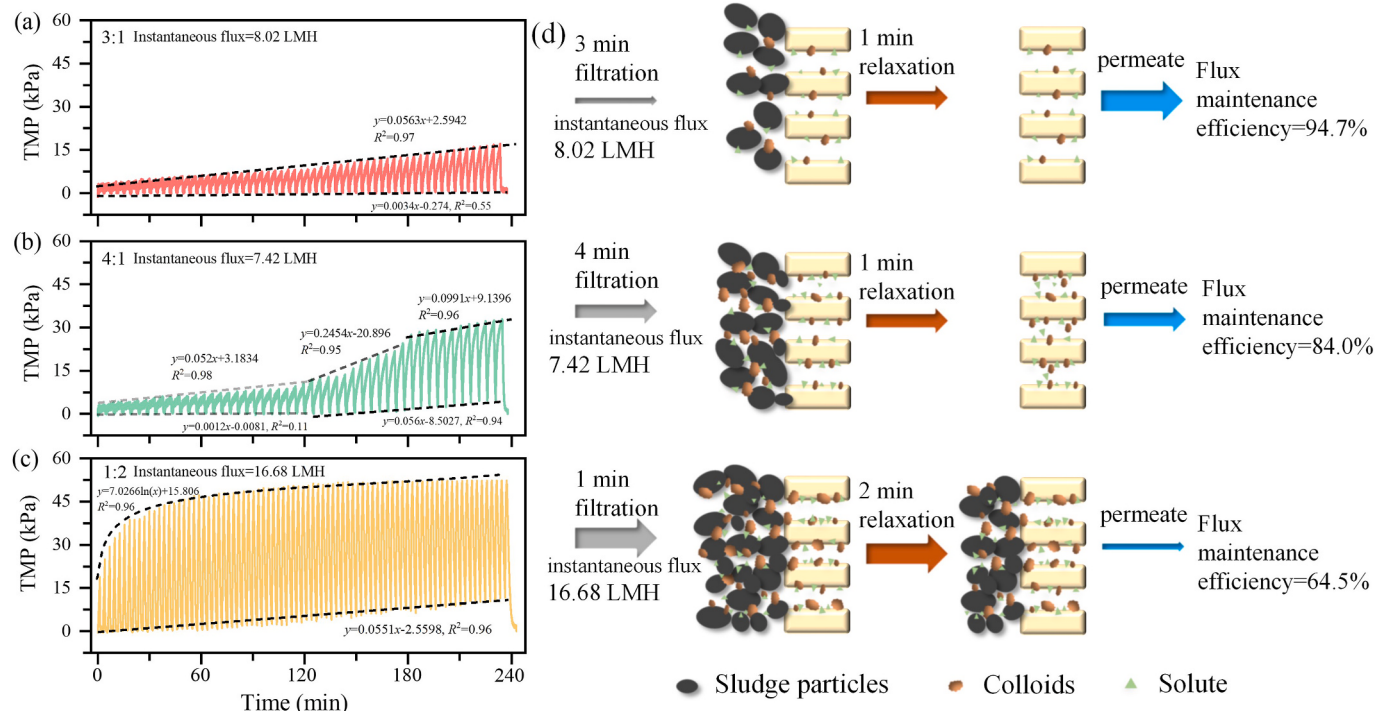


**Fig. 6.** Real-time TMP curves for representative filtration cycles: 3:1 (a), 4:1 (b) and 1:2 (c). Schematic illustration of membrane fouling development (d).

resistance analysis: Although fouling type was inferred from TMP and flux recovery, a resistance-in-series analysis could quantitatively separate reversible and irreversible components. This would enhance mechanistic interpretation and help validate model assumptions (Niu et al., 2024). (3) Empirical model limitations: The power-law model employed here provides a macroscopic fit for TMP evolution but does not incorporate physical fouling parameters such as EPS accumulation, compressibility effects, or biofilm structure. Including these in future models would improve predictive accuracy under varying operational conditions.

Future work should aim to: (1) Validate the 3:1 F/R strategy at pilot scale under real sludge conditions; (2) Integrate online sensors and feedback control to dynamically adjust F/R cycles based on real-time fouling indicators (e.g.,  $\Delta$ TMP slope, permeability loss) (3) Conduct detailed membrane surface analyses (e.g., SEM, FTIR); to correlate model outcomes with physical fouling phenomena (Xing et al., 2025).

In summary, this study offers a low-barrier, scalable approach for fouling mitigation in high-solid AnMBR systems. By focusing on dynamic fouling behavior and process-oriented cycle optimization, it lays the groundwork for future development of intelligent, energy-efficient membrane operation strategies.

#### 4. Conclusions

The high-solid AnMBR (MLTS of  $33.7 \pm 1.0$  g/L) used in this study successfully treated SewS and achieved efficient and stable bioenergy recovery, with values of  $157.8 \pm 15.3$  mL-CH<sub>4</sub>/g-COD<sub>add</sub> and  $258.5 \pm 24.0$  mL-CH<sub>4</sub>/g-VS<sub>add</sub>. The optimal filtration cycle of 3:1 effectively controlled membrane fouling, achieving a low fouling rate of 0.056 kPa/min and the highest FME of 94.7 %. A reliable power-law model was established to describe the relationship between filtrate volume and  $\Delta$ TMP under different filtration cycles:  $\ln(\Delta\text{TMP}) = 0.3018 \ln(v) + 2.3101$ . Furthermore, the membrane fouling type for the 3:1 filtration cycle was identified as intermediate pore blocking using the pore-blocking filtration model. Real-time TMP curves were analyzed to assess the fouling dynamics across representative filtration cycles, providing valuable insights for optimizing filtration processes.

#### CRediT authorship contribution statement

**Hao-Jie Qin:** Writing – review & editing, Writing – original draft, Investigation, Formal analysis, Data curation, Conceptualization. **Ming Zhu:** Writing – review & editing. **Shenghao Ji:** Writing – review & editing. **Ruixin Wu:** Writing – review & editing. **Yuki Yamamoto:** Writing – review & editing, Investigation. **Yu Qin:** Writing – review & editing, Supervision, Resources, Formal analysis, Data curation, Conceptualization. **Yu-You Li:** Writing – review & editing, Supervision, Resources.

#### Declaration of competing interest

The authors declare that they have no known competing financial interests or personal relationships that could have appeared to influence the work reported in this paper.

#### Acknowledgment

This work was supported by the Advanced Graduate School Pioneering Research Support Project for Ph.D. Students (JST SPRING, Grant Number JPMJSP2114). Additionally, it was financially supported by the Grant-in-Aid for Early-Career Scientists (23K13429) and the Grant-in-Aid for Scientific Research (A) (22H00566).

#### Appendix A. Supplementary data

Supplementary data to this article can be found online at <https://doi.org/10.1016/j.jenvman.2025.126659>.

#### Data availability

Data will be made available on request.

## References

- An, Z., Zhu, J., Zhang, M., Zhou, Y., Su, X., Lin, H., Sun, F., 2023. Anaerobic membrane bioreactor for the treatment of high-strength waste/wastewater: a critical review and update. *Chem. Eng. J.* <https://doi.org/10.1016/j.cej.2023.144322>.
- Chen, N., Zhang, X., Qi, L., Gao, F., Wu, G., Li, H., Guo, W., Ngo, H.H., 2025. Enhancement of volatile fatty acids degradation and rapid methanogenesis in a biochar-assisted anaerobic membrane bioreactor via enhancing direct interspecies electron transfer. *J Environ Manage* 380. <https://doi.org/10.1016/j.jenvman.2025.125045>.
- Cheng, H., Li, Y., Kato, H., Li, Y.Y., 2020a. Enhancement of sustainable flux by optimizing filtration mode of a high-solid anaerobic membrane bioreactor during long-term continuous treatment of food waste. *Water Res.* 168, 115195. <https://doi.org/10.1016/j.watres.2019.115195>.
- Cheng, H., Li, Y., Li, L., Chen, R., Li, Y.Y., 2020b. Long-term operation performance and fouling behavior of a high-solid anaerobic membrane bioreactor in treating food waste. *Chem. Eng. J.* 394, 124918. <https://doi.org/10.1016/j.cej.2020.124918>.
- Cheng, H., Qin, H., Li, Y., Guo, G., Liu, J., Li, Y.-Y., 2024. Comparative study of high-performance mesophilic and thermophilic anaerobic membrane bioreactors in the co-digestion of sewage sludge and food waste: methanogenic performance and energy recovery potential. *Sci. Total Environ.* 912, 169518. <https://doi.org/10.1016/j.scitotenv.2023.169518>.
- Fan, J., Chen, Z., Cheng, Y., Ji, H., Hu, C., Qu, J., 2025. Mechanisms and enhancement of hydrogen evolution for membrane anti-fouling and methane upgrading by sacrificed anode in a novel Electro-AnMBR. *Water Res.* 272. <https://doi.org/10.1016/j.watres.2024.122881>.
- Gautam, R.K., Kamilya, T., Verma, S., Muthukumaran, S., Jegathesan, V., Navaratna, D., 2022. Evaluation of membrane cake fouling mechanism to estimate design parameters of a submerged AnMBR treating high strength industrial wastewater. *J Environ Manage* 301. <https://doi.org/10.1016/j.jenvman.2021.113867>.
- Geng, H., Xu, Y., Liu, R., Xu, J., Li, X., Yang, D., Dai, X., 2024. Magnetic porous microspheres altering interfacial thermodynamics of sewage sludge to drive metabolic cooperation for efficient methanogenesis. *Water Res.* 261. <https://doi.org/10.1016/j.watres.2024.122022>.
- Guo, G., Li, Y., Zhou, S., Chen, Y., Qin, Y., Li, Y.Y., 2022. Enhanced degradation and biogas production of waste activated sludge by a high-solid anaerobic membrane bioreactor together with in pipe thermal pretreatment process. *Bioresour. Technol.* 346, 126583. <https://doi.org/10.1016/j.biotech.2021.126583>.
- Guo, G., Zhou, S., Chen, Y., Qin, Y., Huang, X., Li, Y.-Y., 2023. Enhanced methanogenic degradation and membrane fouling associated with protein-EPS by extending sludge retention time in a high-solid anaerobic membrane bioreactor treating concentrated organic sludge. *Water Res.* 248, 120879. <https://doi.org/10.1016/j.watres.2023.120879>.
- Habib, R., Asif, M.B., Iftekhar, S., Khan, Z., Gurung, K., Srivastava, V., Sillanpää, M., 2017. Influence of relaxation modes on membrane fouling in submerged membrane bioreactor for domestic wastewater treatment. *Chemosphere* 181, 19–25. <https://doi.org/10.1016/j.chemosphere.2017.04.048>.
- Hermia, J., 1982. *CONSTANT PRESSURE BLOCKING FILTRATION LAWS: APPLICATION TO POWER-LAW NON-NEWTONIAN FLUIDS*, vol. 60. Transactions of the Institution of Chemical Engineers, pp. 183–187.
- Hu, Y., Du, R., Nitta, S., Ji, J., Rong, C., Cai, X., Qin, Y., Li, Y.Y., 2021. Identification of sustainable filtration mode of an anaerobic membrane bioreactor for wastewater treatment towards low-fouling operation and efficient bioenergy production. *J. Clean. Prod.* 329. <https://doi.org/10.1016/j.jclepro.2021.129686>.
- Jeison, D., van Lier, J.B., 2006. Cake layer formation in anaerobic submerged membrane bioreactors (AnSMBR) for wastewater treatment. *J Membr Sci* 284, 227–236. <https://doi.org/10.1016/j.memsci.2006.07.035>.
- Jiang, M., Huang, J., Li, P., Ataa, B., Gu, J., Wu, Z., Qiao, W., 2023. Optimization of membrane filtration and cleaning strategy in a high solid thermophilic AnMBR treating food waste. *Chemosphere* 342. <https://doi.org/10.1016/j.chemosphere.2023.140151>.
- Kwon, Y., Park, J., Kim, G.B., Jo, Y., Park, S., Kim, S.H., 2023. Anaerobic digestion of sewage sludge using anaerobic dynamic membrane bioreactor under various sludge composition and organic loading rates. *Bioresour. Technol.* 384. <https://doi.org/10.1016/j.biotech.2023.129275>.
- Lei, Z., Yang, S., Li, X., Wen, W., Huang, X., Yang, Y., Wang, X., Li, Y.Y., Sano, D., Chen, R., 2019. Revisiting the effects of powdered activated carbon on membrane fouling mitigation in an anaerobic membrane bioreactor by evaluating long-term impacts on the surface layer. *Water Res.* 167. <https://doi.org/10.1016/j.watres.2019.115137>.
- Li, L., Bu, Y., Feng, W., Kubota, K., Pan, Y., Huang, Y., Li, Y.Y., Qin, Y., 2024. Biomethane recovery and prokaryotic shifts in anaerobic co-digestion of food waste and paper waste in organic fraction of municipal solid waste: effect of paper content. *Bioresour. Technol.* 406. <https://doi.org/10.1016/j.biotech.2024.130964>.
- Liang, M., Chen, J., Li, Q., Wu, X., Zheng, M., Zan, F., Chen, G., 2025. Deep insight of the efficiency and fouling mechanisms in reciprocating and biogas sparging anaerobic membrane bioreactor for food waste digestion. *Chem. Eng. J.* 518. <https://doi.org/10.1016/j.cej.2025.164391>.
- Lin, H., Peng, W., Zhang, M., Chen, J., Hong, H., Zhang, Y., 2013. A review on anaerobic membrane bioreactors: applications, membrane fouling and future perspectives. *Desalination*. <https://doi.org/10.1016/j.desal.2013.01.019>.
- Liu, J., Zheng, J., Zhang, J., Yu, D., Wei, Y., 2020. The performance evaluation and kinetics response of advanced anaerobic digestion for sewage sludge under different SRT during semi-continuous operation. *Bioresour. Technol.* 308. <https://doi.org/10.1016/j.biotech.2020.123239>.
- Liu, Y., Xi, Y., Li, Q., Dzakpasu, M., Chen, R., Li, Y.Y., 2024. Biokinetic and microbial insights into regulatory mechanisms of long-chain fatty acid degradation during food waste-lipid co-digestion within anaerobic membrane bioreactor. *Bioresour. Technol.* 408. <https://doi.org/10.1016/j.biotech.2024.131223>.
- Liu, Y., Zhang, H., Jiang, C., Jiang, X., Sakamaki, T., Li, X., 2023. Effect of bio-electrochemical systems on the removal of organic and inorganic membrane fouling from anaerobic membrane bioreactors. *Sep. Purif. Technol.* 312. <https://doi.org/10.1016/j.seppur.2023.123395>.
- Maqbool, T., Khan, S.J., Lee, C.H., 2014. Effects of filtration modes on membrane fouling behavior and treatment in submerged membrane bioreactor. *Bioresour. Technol.* 172, 391–395. <https://doi.org/10.1016/j.biotech.2014.09.064>.
- Meng, F., Chae, S.R., Drews, A., Kraume, M., Shin, H.S., Yang, F., 2009. Recent advances in membrane bioreactors (MBRs): membrane fouling and membrane material. *Water Res.* 43, 1489–1512. <https://doi.org/10.1016/j.watres.2008.12.044>.
- Niu, C., Pan, Y., Lu, X., Wang, S., Zhang, Z., Zheng, C., Tan, Y., Zhen, G., Zhao, Y., Li, Y., 2020. Mesophilic anaerobic digestion of thermally hydrolyzed sludge in anaerobic membrane bioreactor: Long-Term performance, microbial community dynamics and membrane fouling mitigation. *J Memb Sci* 612. <https://doi.org/10.1016/j.memsci.2020.118264>.
- Niu, C., Zhang, Z., Cai, T., Pan, Y., Lu, X., Zhen, G., 2024. Sludge bound-EPS solubilization enhance CH4 biocconversion and membrane fouling mitigation in electrochemical anaerobic membrane bioreactor: insights from continuous operation and interpretable machine learning algorithms. *Water Res.* 264. <https://doi.org/10.1016/j.watres.2024.122243>.
- Park, J., Cayetano, R.D.A., Kwon, Y., Kim, G.B., Jo, Y., Kim, S.H., 2023. Improved sludge anaerobic digestion capacity by dynamic membrane and alkaline-thermal pretreatment: Long-term continuous operation and techno-economic analysis. *Chem. Eng. J.* 474. <https://doi.org/10.1016/j.cej.2023.145735>.
- Qin, H., Liu, Jianmin, Chao, W., Liu, Jianyong, Chang, S., Chang, C.-T., Martins, T., Li, Y.-Y., Cheng, H., 2025. Membrane-enhanced methanogenesis efficiency and biomass retention in EGSB-AnMBR for food waste press filtrate treatment. *Environ. Res.* 281, 121978. <https://doi.org/10.1016/j.enrev.2025.121978>.
- Qin, Y., Zhu, A., Wu, J., Li, L., Hojo, T., Kubota, K., Li, Y.Y., 2024. Mass flow and microbial shifts in recirculated two-phase anaerobic digestion for biohythane production: effect of hydraulic retention time. *J. Clean. Prod.* 468. <https://doi.org/10.1016/j.jclepro.2024.143092>.
- Raposo, F., De La Rubia, M.A., Fernández-Cegrí, V., Borja, R., 2012. Anaerobic digestion of solid organic substrates in batch mode: an overview relating to methane yields and experimental procedures. *Renew. Sustain. Energy Rev.* <https://doi.org/10.1016/j.rser.2011.09.008>.
- Rong, C., Wang, T., Luo, Z., Hu, Y., Kong, Z., Qin, Y., Hanaoka, T., Ito, M., Kobayashi, M., Li, Y.Y., 2022. Pilot plant demonstration of temperature impacts on the methanogenic performance and membrane fouling control of the anaerobic membrane bioreactor in treating real municipal wastewater. *Bioresour. Technol.* 354. <https://doi.org/10.1016/j.biotech.2022.127167>.
- Song, L., Ye, M., Wang, C., Ren, Y., Li, D., Ha, J., Qin, Y., Li, Q., Niu, Q., Li, Y.Y., 2024. Methanogenic degradation of long-chain fatty acids associated with syntrophic microbial dynamics during thermophilic AnMBR treatment of lipid-rich dairy wastes. *Chem. Eng. J.* 498. <https://doi.org/10.1016/j.cej.2024.155702>.
- Sreedhar, N., Mavukkandy, M.O., Aminabhavi, T.M., Hong, S., Arafat, H.A., 2022. Fouling mechanisms in ultrafiltration under constant flux: effect of feed spacer design. *Chem. Eng. J.* 446. <https://doi.org/10.1016/j.cej.2022.136563>.
- Tan, Y., Xiao, Y., Hao, T., 2024. Carbon fixation via volatile fatty acids recovery from sewage sludge through electrochemical-pretreatment-based anaerobic digestion. *Water Res.* 258. <https://doi.org/10.1016/j.watres.2024.121736>.
- Wang, C., Ding, M., Ng, T.C.A., Ng, H.Y., 2023a. Mechanistic insights into simultaneous reversible and irreversible membrane fouling control in a vibrating anaerobic membrane bioreactor for sustainable municipal wastewater treatment. *Chem. Eng. J.* 466. <https://doi.org/10.1016/j.cej.2023.143226>.
- Wang, M., Ren, T., Yin, M., Lu, K., Xu, H., Huang, X., Zhang, X., 2023b. Enhanced anaerobic wastewater treatment by a binary electroactive material: Pseudocapacitance-conductance-mediated microbial interspecies electron transfer. *Environ. Sci. Technol.* 57, 12072–12082. <https://doi.org/10.1021/acs.est.3c01986>.
- Wu, M., Zhong, H., Lin, H., Zhao, P., Song, W., Wang, X., 2025. Novel insights into fouling mechanisms in anaerobic acidification membrane bioreactor: the leading role of pH value. *Sep. Purif. Technol.* 357. <https://doi.org/10.1016/j.seppur.2024.130219>.
- Wu, Z.L., Lin, Z., Sun, Z.Y., Gou, M., Xia, Z.Y., Tang, Y.Q., 2020. A comparative study of mesophilic and thermophilic anaerobic digestion of municipal sludge with high-solids content: reactor performance and microbial community. *Bioresour. Technol.* 302, 122851. <https://doi.org/10.1016/j.biotech.2020.122851>.
- Xing, F., Wang, S., Wang, T., Sun, B., Meng, H., 2025. Comprehensive performance of a new-type hybrid membrane bioreactor applied to mainstream anammox process. *J Environ Manage* 373. <https://doi.org/10.1016/j.jenvman.2024.123771>.
- Xu, H., Xiao, K., Wang, X., Liang, S., Wei, C., Wen, X., Huang, X., 2020. Outlining the roles of membrane-foulant and foulant-foulant interactions in organic fouling during microfiltration and ultrafiltration: a mini-review. *Front. Chem.* <https://doi.org/10.3389/fchem.2020.00417>.
- Yang, X., Lei, Z., Wang, L., Chen, R., 2024. A deeper investigation of membrane fouling in anaerobic membrane bioreactors for wastewater treatment: influencing factors and fouling layer characteristics. *J Environ Manage* 371. <https://doi.org/10.1016/j.jenvman.2024.123223>.
- Ye, M., Sun, B., Song, L., Qin, Y., Luo, J., Zhu, A., Li, Y.Y., 2023. Organic transformation, lactic acid metabolism, and membrane performance in high-rate methanogenic treatment of dairy processing wastewater using thermophilic high-solid anaerobic

- membrane bioreactor. *Chem. Eng. J.* 455, 140780. <https://doi.org/10.1016/j.cej.2022.140780>.
- Ye, M., Zhu, A., Liu, J., Li, Y.Y., 2024. Iron recycle-driven organic capture and sidestream anaerobic membrane bioreactor for revolutionizing bioenergy generation in municipal wastewater treatment. *Environ. Sci. Technol.* 58, 9350–9360. <https://doi.org/10.1021/acs.est.3c10954>.
- You, Y., Guo, J., Jiang, J., 2025. Insight into the performance and fouling characteristics of submerged ceramic membrane bioreactor in wastewater treatment. *J Environ Manage* 373. <https://doi.org/10.1016/j.jenvman.2024.123900>.
- Zhang, J.X., Li, Y.S., Du, W.J., Tian, T., Xuan, L., Yu, H.Q., 2025. Driving force shapes the biocake characteristics in membrane-based bioreactors. *Water Res.* 268. <https://doi.org/10.1016/j.watres.2024.122592>.
- Zhang, W., Liang, W., Zhang, Z., Hao, T., 2021. Aerobic granular sludge (AGS) scouring to mitigate membrane fouling: performance, hydrodynamic mechanism and contribution quantification model. *Water Res.* 188. <https://doi.org/10.1016/j.watres.2020.116518>.
- Zhu, M.C., Wang, J.W., Lu, Y.Z., Hu, Z.X., Chen, S.W., Li, N., 2025. Enhancement of membrane filtration performance and mitigation of sludge calcification in an intermittent anaerobic membrane bioreactor treating high-calcium wastewater. *Sep. Purif. Technol.* 354. <https://doi.org/10.1016/j.seppur.2024.129028>.